Leakage Fault Identification in a Hydraulic Positioning System Using Extended Kalman Filter

L. An
Graduate Research Assistant

N. Sepehri*
Professor

Department of Mechanical and Industrial Engineering
The University of Manitoba, Winnipeg, MB, Canada R3T 5V6

Abstract-This paper presents the application of extended Kalman filter (EKF) towards leakage fault identification in a servo-hydraulic actuation system. The EKF rebuilds information about the system's states based on the input signal and measurements of the actuator displacement and cylinder chamber pressures. By comparing the estimated states with the measured ones, residual signals are generated. When faults happen, the levels of certain residual errors change. It is shown that different leakage types could cause changes in different residual errors; thus, the EKF-based method has the potential to identify fault types. Experiments show that EKF estimator promptly and reliably responds to faults caused by different actuator leakages. With the mapping of residual error changes, the EKF successfully identifies cross-port (internal) leakage, as well as cylinder chamber (external) leakage at either side of the actuator.

1. INTRODUCTION

Due to the application areas, tough working conditions and complexity of fluid power circuits, mechanical faults such as components wear, leakage, seal damage and other malfunctioning in hydraulic systems, can cause serious consequences and sometimes casualties. Among the common faults associated with hydraulic systems is the leakage of hydraulic fluid. Leakage can be classified into two types according to its location: internal and external. If the fluid leaks to another part of the fluid circulation within the hydraulic system, it is considered as internal leakage. If the fluid leaks outside of the fluid circulation or the leaked hydraulic fluid is collected by the reservoir, it is classified as external leakage. The main cause of leakage is the wear of the valves, pistons and other moving component [1]. The focus of this paper is on the leakage happening within the actuator. Two types of leakage are under consideration: external leakage on either side of the actuator cylinder, and internal (cross-port) leakage between the two chambers of the actuator cylinder.

System fault detection and isolation (FDI) has been developed in the past decade. A detailed survey on existing FDI techniques has been summarized researchers [2][3]. However, FDI in hydraulic systems is difficult to implement in practice due to its inherent nonlinearities. Mathematical tools for linear systems such as autoregressive models with forgetting factors have been under inspection by some researcher [1][4] in hydraulic FDI. But the applications of these methods have been limited. Artificial neural networks (ANN) have also been considered due to their effectiveness in mapping nonlinear dynamics [5][6]. ANN shows its grace as a mathematical tool in pattern recognition but it also has drawbacks in convergence and local optimum. Apart from parametric methods, schemes based on state space model such as the nonlinear observers [7][8] have also been under consideration have been developed. Compared to these methods, the application of Kalman filter in the field of FDI is relatively new [9]. Due to the computational difficulties, Kalman filter has been widely applied only after the rapid development of computers [10]. For nonlinear applications, the extended Kalman filter (EKF) has been developed. Successful application of EKF towards FDI in hydraulic systems has been reported [9][11].

In this paper we explore, for the first time, the development of a FDI scheme using EKF method to identify leakage faults in a servo-hydraulic positioning system. Leakage faults on either side, or between the two chambers of the actuator cylinder are considered. By comparing the actual state with corresponding estimation from EKF, a pattern map of the change of the residual errors is obtained according to the experiments. It is shown that cross-port leakage as well as external leakage at either side of the actuator can be successfully identified.

2. EXPERIMENTAL TEST RIG

The experimental setup is shown in Fig. 1.

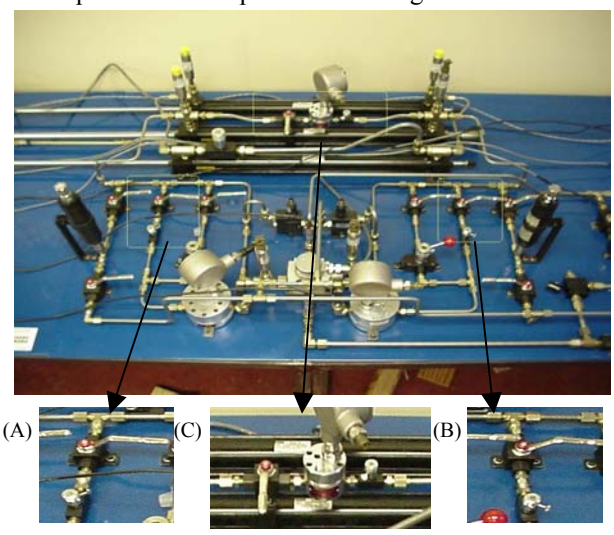

Fig. 1: Hydraulic test station.

* Corresponding author; email: nariman@cc.umanitoba.ca

The test rig, consisting of a double-rod actuator, is powered by a motor-driven hydraulic pump. The Moog D765 servovalve controls the movement of the actuator. All control/diagnosis algorithms are implemented on a high speed PC equipped with data acquisition board and encoder card. The subplots of (A), (B) and (C) in Fig.1 show the details of the bypasses and valves for generating the external leakage (A and B), and the internal leakage (C).

3. SYSTEM MODEL

3.1 Nonlinear model

With reference to Fig. 2, the flow equations of the servovalve is represented as [12]:

$$\begin{cases} q_i = C_d w x_{sp} \sqrt{\frac{2}{\rho}(p_s - p_i)} \\ q_o = C_d w x_{sp} \sqrt{\frac{2}{\rho}(p_o - p_e)} \end{cases} (x_{sp} > 0) \quad (1a)$$

$$\begin{cases} q_i = C_d w x_{sp} \sqrt{\frac{2}{\rho}(p_i - p_e)} \\ q_o = C_d w x_{sp} \sqrt{\frac{2}{\rho}(p_s - p_o)} \end{cases} (x_{sp} < 0) \quad (1b)$$

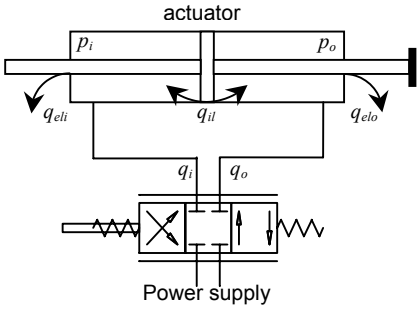

Fig. 2: Schematic of hydraulic test station.

where q_i and q_o are the inlet flow and the outlet flow of the servovalve, respectively. p_s and p_e are pump and return pressures. p_i is pressure in inlet (left) side of the actuator cylinder, and p_o is the pressure in outlet (right) side of the actuator cylinder. x_{sp} is the servovalve spool displacement. C_d is the orifice coefficient of discharge, and w is the orifice area gradient. ρ is the density of the hydraulic oil.

Continuity equations for the hydraulic flow going out and into the actuator are

$$\begin{cases} q_i = A_i \dot{x} + \frac{1}{\beta} V_i(x) \dot{p}_i + q_{il} + q_{eli} \\ q_o = A_o \dot{x} - \frac{1}{\beta} V_o(x) \dot{p}_o + q_{il} - q_{elo} \end{cases} \quad (2)$$

where β is the effective bulk modulus of the hydraulic fluid. A_i and A_o are the piston areas (note: for the experimental test rig under investigation $A_i = A_o$). $V_i(x)$ and $V_o(x)$ are the volumes of fluid trapped at the sides of the actuator, given by the following equations:

$$\begin{cases} V_i(x) = V_i^0 + A_i(x - X_{\min}) \\ V_o(x) = V_o^0 + A_o(X_{\max} - x) \end{cases} \quad (3)$$

In which V_i^0, V_o^0 are volumes of fluid trapped in the supply pipes, inlet side and outlet side respectively. $X_{\min}$, $X_{\max}$ are the positions of the ram in fully retracted and fully extended mode, respectively. q_{il}, q_{eli} and q_{elo} are the internal (cross-port) leakage and the external leakage at p_i or p_o sides of the cylinder (see Fig. 2).

The dynamics of the servovalve is expressed as a typical second-order system between the spool displacement, x_{sp}, and the input voltage, u, to the valve:

$$u = \frac{1}{k_{sp}\omega_n^2}\ddot{x}_{sp} + \frac{2d_m}{k_{sp}\omega_n}\dot{x}_{sp} + \frac{1}{k_{sp}}x_{sp} \quad (4)$$

ω_n is the natural frequency, and k_{sp} is the DC gain and d_m is the damping ratio. The dynamic equation of the actuator is:

$$m_a \ddot{x} = (p_i A_i - p_o A_o) - F_c \quad (5)$$

where m_a is the mass of the ram, and F_c denotes the effective friction. After series of experiments on the test station, the improved Karnopp model is adopted to model the friction in the hydraulic actuator under investigation.

$$\begin{cases} F_c(\dot{x}) = f_{sl} + (f_{st} - f_{sl}) \cdot e^{-\frac{|\dot{x}|}{a}} \cdot \mathrm{sgn}(\dot{x}) + d\dot{x} & |\dot{x}| > v_\circ \\ F_c(\dot{x}) = f_{st} \cdot \mathrm{sgn}(\dot{x}) & |\dot{x}| \le v_\circ \end{cases} \quad (6)$$

where f_{st} and f_{sl} are the static and slip frictions, respectively. a is the decay ratio of the slip friction, d is the effective damping ratio, while $v_\circ$ is the threshold for break away velocity for switching between static friction and slip friction. sgn(·) is expressed as $\{ \mathrm{sgn}(\dot{x}) = \dot{x}/|\dot{x}|, |\dot{x}| \neq 0;\ \mathrm{sgn}(\dot{x}) \in [-1, 1],\ \dot{x} = 0 \}$.

3.2 State space model

Choosing the state vector $\vec{\mathbf{x}} = [x_1, x_2, x_3, x_4, x_5, x_6]^T = [x_{sp}, p_i, p_o, x, \dot{x}, \dot{x}_{sp}]^T$, the state space model for the hydraulic system is

$$\dot{x}_1 = x_6 \quad (7a)$$

$$\dot{x}_2 = \begin{cases} \frac{\beta}{V_i(x_4)}[C_d w x_1 \sqrt{\frac{2}{\rho}(p_s - x_2)} - A_i x_5] & (x_1 > 0) \\ \frac{\beta}{V_i(x_4)}[C_d w x_1 \sqrt{\frac{2}{\rho}(x_2 - p_e)} - A_i x_5] & (x_1 < 0) \end{cases} \quad (7b)$$

$$\dot{x}_3 = \begin{cases} \dfrac{\beta}{V_o(x_4)}[-C_d w x_1 \sqrt{\dfrac{2}{\rho}(x_3 - p_e)} + A_o x_5] (x_1 > 0) \\ \dfrac{\beta}{V_o(x_4)}[-C_d w x_1 \sqrt{\dfrac{2}{\rho}(p_s - x_3)} + A_o x_5] (x_1 < 0) \end{cases} \quad (7c)$$

$$\dot{x}_4 = x_5 \quad (7d)$$

$$\dot{x}_5 = \frac{1}{m_a}(A_i x_2 - A_o x_3 - F_c(x_5)) \quad (7e)$$

$$\dot{x}_6 = -2d_m \omega_n x_6 - \omega_n^2 x + k_{sp} \omega_n^2 u \quad (7f)$$

where $F_c(\cdot)$ is calculated from (6) and the state variable x_5 is the actuator velocity. Note that the leakage flows are not considered in the system space model.

To meet the requirement of digital computing, above state space representation is discretized using the forward difference method. *T* represents the sampling time in actual applications

$$x_1(k) = T x_6(k-1) + x_1(k-1) \quad (8a)$$

$$x_2(k) = \begin{cases} \dfrac{T\beta}{V_i(x_4(k-1))}[C_d w x_1(k-1) \\ \sqrt{\dfrac{2}{\rho}(p_s - x_2(k-1))} - A_i x_5(k-1)] \\ + x_2(k-1) \quad (x_1(k-1) > 0) \\ \dfrac{T\beta}{V_i(x_4(k-1))}[C_d w x_1(k-1) \\ \sqrt{\dfrac{2}{\rho}(x_2(k-1) - p_e)} - A_i x_5(k-1)] \\ + x_2(k-1) \quad (x_1(k-1) \le 0) \end{cases} \quad (8b)$$

$$x_3(k) = \begin{cases} \dfrac{T\beta}{V_o(x_4(k-1))}[-C_d w x_1(k-1) \\ \sqrt{\dfrac{2}{\rho}(x_3(k-1) - p_e)} + A_o x_5(k-1)] \\ + x_3(k-1) \quad (x_1(k-1) > 0) \\ \dfrac{T\beta}{V_o(x_4(k-1))}[-C_d w x_1(k-1) \\ \sqrt{\dfrac{2}{\rho}(p_s - x_3(k-1))} + A_o x_5(k-1)] \\ + x_3(k-1) \quad (x_1(k-1) \le 0) \end{cases} \quad (8c)$$

$$x_4(k) = T x_5(k-1) + x_4(k-1) \quad (8d)$$

$$x_5(k) = \frac{T}{m_a}(A_i x_2(k-1) - A_o x_3(k-1) - F_c(x_5(k-1)) + x_5(k-1) \quad (8e)$$

$$x_6(k) = T[-2d_m \omega_n x_6(k-1) - \omega_n^2 x(k-1) + k_{sp} \omega_n^2 u(k)] + x_6(k-1) \quad (8f)$$

4. FDI ALGORITHM

4.1 EKF scheme

The basic concept of the EKF scheme is to linearize the estimation of the actual system around the current estimate, using partial derivatives of the process and measurements to compute posteriori estimates. Consider a nonlinear system represented by a stochastic difference equation

$$\begin{cases} \mathbf{x}_k = \mathbf{f}(\mathbf{x}_{k-1}, \mathbf{u}_k, \mathbf{w}_{k-1}) \\ \mathbf{y}_k = \mathbf{h}(\mathbf{x}_k, \mathbf{v}_k) \end{cases} \quad (9)$$

The linearized representation of this nonlinear system is written as

$$\begin{cases} \mathbf{x}_k \approx \tilde{\mathbf{x}}_k + \mathbf{A}(\mathbf{x}_{k-1} - \hat{\mathbf{x}}_{k-1}) + \mathbf{W}\mathbf{w}_{k-1} \\ \mathbf{y}_k \approx \tilde{\mathbf{y}}_k + \mathbf{H}(\mathbf{x}_k - \tilde{\mathbf{x}}_k) + \mathbf{V}\mathbf{v}_k \end{cases} \quad (10)$$

where $\mathbf{x}_k$ and $\mathbf{y}_k$ are the vectors of the actual state and the output, $\hat{\mathbf{x}}$ is the posteriori estimation of the states, $\tilde{\mathbf{x}}_k$ and $\tilde{\mathbf{y}}_k$ are the vectors of the approximated state and measurements given by the following approximating equation:

$$\begin{cases} \tilde{\mathbf{x}}_k = \mathbf{f}(\hat{\mathbf{x}}_{k-1}, \mathbf{u}_k, \mathbf{0}) \\ \tilde{\mathbf{y}}_k = \mathbf{h}(\tilde{\mathbf{x}}_k, \mathbf{0}) \end{cases} \quad (11)$$

A, **W**, **H**, and **V** are the Jacobian matrices given by

$$\mathbf{A}_{[i,j]} = \left.\frac{\partial f_i}{\partial x_j}\right|_{(\hat{\mathbf{x}}_k, \mathbf{u}_k, 0)}; \quad \mathbf{W}_{[i,j]} = \left.\frac{\partial f_i}{\partial w_j}\right|_{(\hat{\mathbf{x}}_k, \mathbf{u}_k, 0)}$$

$$\mathbf{H}_{[i,j]} = \left.\frac{\partial h_i}{\partial x_j}\right|_{(\hat{\mathbf{x}}_k, 0)}; \quad \mathbf{V}_{[i,j]} = \left.\frac{\partial f_i}{\partial v_j}\right|_{(\hat{\mathbf{x}}_k, 0)} \quad (12)$$

∂f and ∂h represent for the elements in nonlinear state representation **f** and **h**, respectively. The complete EKF algorithm can be grouped into two stages as shown in the following:

(i): time update equations

$$\begin{cases} \hat{\mathbf{x}}_k^- = \mathbf{f}(\hat{\mathbf{x}}_{k-1}, \mathbf{u}_k, \mathbf{0}) \\ \hat{\mathbf{P}}_k^- = \mathbf{A}_k \mathbf{P}_{k-1} \mathbf{A}_k^T + \mathbf{W}_k \mathbf{Q}_{k-1} \mathbf{W}_k^T \end{cases} \quad (13)$$

(ii): measurement update equations

$$\begin{cases} \mathbf{K}_k = \mathbf{P}_k^- \mathbf{H}_k^T (\mathbf{H}_k \mathbf{P}_k^- \mathbf{H}_k^T + \mathbf{V}_k \mathbf{R}_k \mathbf{V}_k^T)^{-1} \\ \hat{\mathbf{x}}_k = \hat{\mathbf{x}}_k^- + \mathbf{K}_k(\mathbf{y}_k - \mathbf{h}(\hat{\mathbf{x}}_k^-, \mathbf{0})) \\ \mathbf{P}_k = (\mathbf{I} - \mathbf{K}_k \mathbf{H}_k)\mathbf{P}_k^- \end{cases} \quad (14)$$

Note that Jacobian matrices are updated in EKF at each step sample '*k*' due to the requirement of linearization. The measurement and process noise covariance matrices are also considered to be changing at each step. In this paper, the covariance matrices are set to the following values:

$$\mathbf{W} = diagnal\begin{bmatrix} 10^{-20} & 10^4 & 10^4 & 10^{-6} & 10^{-4} & 10^{-20} \end{bmatrix}$$

$$\mathbf{V} = diagnal\begin{bmatrix} 10^{-4} & 10^5 & 10^5 \end{bmatrix}$$

4.2 Residual generation

Under normal operating condition, the output vector of the EKF estimator, $\hat{\mathbf{x}}_k$, converges to the actual system state

vector, $\mathbf{x}_k$, with each sampling such that all elements of the residual error vector, $\mathbf{e}_k$, remain relatively low. The residual errors during normal condition reflect the estimation errors. However, when fault occurs, one or more of the system parameters changes, i.e., the dynamic feature of the system changes. A structural discrepancy lies between the faulty system and the EKF estimator. Due to this discrepancy, the estimation of the EKF on certain elements of the system state vector diverges from the actual state trajectory.

With reference to Fig. 3, the ram displacement, x, and actuator chamber pressures, P_i and P_o, are measured. The EKF estimator accepts the system input u and these measurements and produces estimation on all system state variables [see equation (8)]. The residual errors of the chamber pressures, P_i and P_o, are then calculated and the moving average values of the errors are obtained to smooth out the effect of noise. By observing the variation of the moving average of the errors on the chamber pressures, external and cross-port leakage are identified.

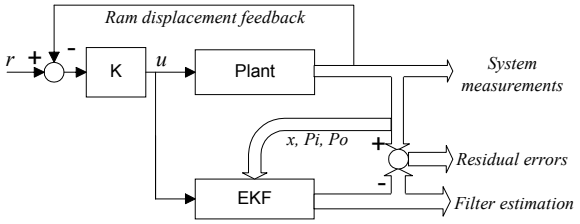

Fig. 3: EKF-based FDI system block diagram

5. EXPERIMENTAL RESULTS

In the experiments, the test rig worked in closed-loop, under a simple proportional controller. The supply pressure was set to 2000 psi. Other parameters of the station are listed in Table 1.

Table 1: Hydraulic test station parameters.

A_i A_o (m^2)	6.33×10^{-4}	k_{sp}	2.794×10^{-5}
M_a (kg)	10.0	ω_n (rad/s)	200.0π
$X_{\min}$ (m)	0.0	d_m	0.7
$X_{\max}$ (m)	0.6096	V_i^0 (m^3)	2.14×10^{-5}
d (Ns/m)	1.0×10^{3}	V_o^0 (m^3)	2.14×10^{-5}

In each experiment the actuator was commanded to follow a 10cm sinusoidal displacement with frequency of 1Hz around its midpoint position. Both external leakages (P_i or P_o, sides) and internal (cross-port) leakage were introduced into the system by tuning the opening of the bleed valves mounted on corresponding bypasses [see insets (A), (B) and (C) in Fig. 2]. All faults occurred around the 5th second after the actuator was started. Only single fault mode was tested at a time. The initial value of the state vector for EKF was set to $\mathbf{x}=[0,6.8\times10^6, 6.8\times10^6, 0, 0, 0]^T$ for all tests.

Fig 4 shows the control signal and the displacement response pertaining to the first test. In this test, an abrupt external leakage was made on the *Pi* side of the actuator. The leakage flow is shown in Fig. 5. The leaking flow was ≈0.15 gal/min. Figs. 6 and 7 show the plots of measured and estimated cylinder chamber pressures, P_i and P_o, and corresponding moving average errors. It is seen that, in the absence of leakage fault, both estimates closely match the actual variation of the cylinder pressures and the residual errors quickly converge and stay at relatively low levels (≈10% of the actual values). When the leakage at the P_i side occurred, the residual error of chamber pressure P_i increased significantly by 50%, while the residual error of chamber pressure P_o did not change. This unique feature is an effective indication to the occurrence of leakage fault at the inlet chamber of P_i.

The next experiment involved a further increase of the leakage level at the P_i side (to ≈0.28gal/min). Fig. 8 shows the plot of the leakage. Figure 9 shows the plots of the moving average errors for both P_i and P_o. According to Fig. 9, the increase of the residual error of the chamber pressure on P_i side is 80% of the normal level, while the residual error of the P_o remain the same.

Due to the symmetric structure of the cylinder and the servovalve, the residual error pertaining estimation of the chamber pressure at the P_i side remains the same, while the residual error of the P_o estimation changes with the amount of leakage. With reference to Figs. 10 and 11, it can be seen that the residual error of chamber pressure P_o increased by 20% due to the occurrence of leakage (Fig. 10). It is also seen (Fig. 11) that the higher the leakage the higher the change in the P_o residual error (≈100%).

The response of the EKF estimator to the cross-port leakage between the cylinder chambers [see inset (C) in Fig. 1] was also experimentally tested. When a leakage flow of ≈1.9gal/min was applied (Fig. 12a), both residual errors of the two chamber pressures increased. This clearly identifies the internal leakage from the external leakage faults. When a higher internal leakage (Fig. 12b) was introduced, both residual errors increased further (more than those in Fig. 13). The following table summarizes the identification pattern.

Table 2: Leakage identification mapping.

Residual	External Leakage, P_i side	External Leakage, P_o side	Internal Leakage
P_i	Increases	No change	Increases
P_o	No change	Increases	Increases

6. CONCLUSIONS

This study clearly demonstrated that, extended Kalman filter (EKF) when using a combined model of nonlinear dynamics with friction, can closely simulate the states of an electrohydraulic positioning system. With limited inputs, the EKF estimator successfully identified three different leakage faults in a hydraulic actuator. A residual generation strategy was proposed and was tested in experiments. According to the residual errors, different patterns of change are obtained which can be used to identify different leakage levels. Also, it was shown that the magnitudes of

the corresponding residual errors increase proportionally with the changes in the leakage faults.

REFERENCES

[1] Skormin, V.A.; Apone, J.; On-line diagnostics of a variable displacement pump of a flight actuation system; Proceedings of the IEEE 1995 National Aerospace and Electronics Conference, NAECON, Vol.: 1; pp. 503 –510; 22-26 May 1995.

[2] R. Isermann, Supervision, Fault-Detection and Fault-Diagnosis Methods – An Introduction, Control Eng. Practice, Vol. 5, No. 5, pp. 639-652; 1997.

[3] Frank, Paul M., On-line fault detection in uncertain nonlinear systems using diagnostic observers: a survey, INT. J. SYSTEMS SCI. Vol.25, No.12, pp. 2129-2154, 1994.

[4] McCormick, A.C., Nandi, A.K., Jack, L.B., Application of periodic time-varying autoregressive models to the detection of bearing faults, Proceedings of the Institution of Mechanical Engineers, Part C: Journal of Mechanical Engineering Science, Vol. 212, No. 6, pp. 417-428; 1998.

[5] He, S.; Sepehri, N., Online modeling and prediction of a hydraulic force-acting system using neural networks, Systems, Man, and Cybernetics, 2000 IEEE International Conference, Volume: 4 , pp. 2667 –2672; 2000.

[6] Snider, L.A.; Yuen Yee Shan, The artificial neural networks based relay algorithm for distribution system high impedance fault detection, Advances in Power System Control, Operation and Management, APSCOM-97. Fourth International Conference, Volume: 1, pp. 100 –106; 1997.

[7] Frank, Paul M; On-line fault detection in uncertain nonlinear system using diagnostic observers: a survey, , Int. Journal of system science, Vol. 25, No. 12, pp. 2129-2154; 1994.

[8] Yang, H.; Saif, M., Monitoring and diagnostics of a class of nonlinear systems using a nonlinear unknown input observer, Control Applications, Proceedings of the 1996 IEEE International Conference, pp. 1006 –1011; 1996.

[9] Khoshzaban, M.; Sassani, F.; Lawrence, P.D., Online state and parameter estimation of an electrohydraulic valve for intelligent monitoring, Advanced Intelligent Mechatronics '97. Final Program and Abstracts., IEEE/ASME International Conference, pp. 141-146; 1997.

[10] Haykin, S.; Kalman filtering and neural networks, John Wiley & Sons, Inc. New York, N.Y. 2001

[11] An, L., Sepehri, N.; Hydraulic actuator circuit fault detection using extended Kalman filter, Proceedings of the American Control Conference, pp. 4261-4266, 2003.

[12] Merrit, H. E.,Hydraulic Control Systems, Wiley, New York, 1967.

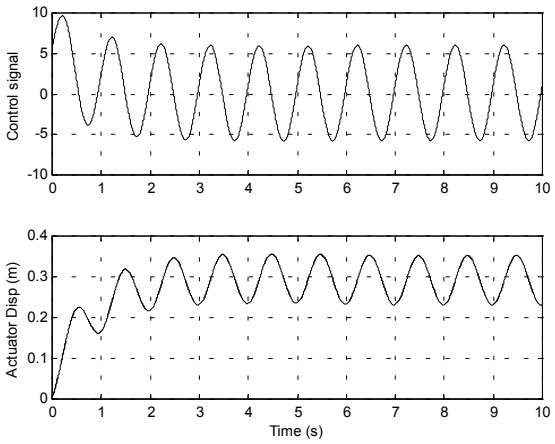

Figure 4: Control signal and actuator displacement

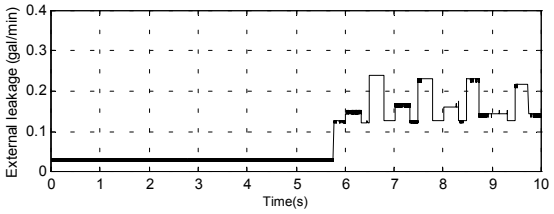

Figure 5: External leakage, level I

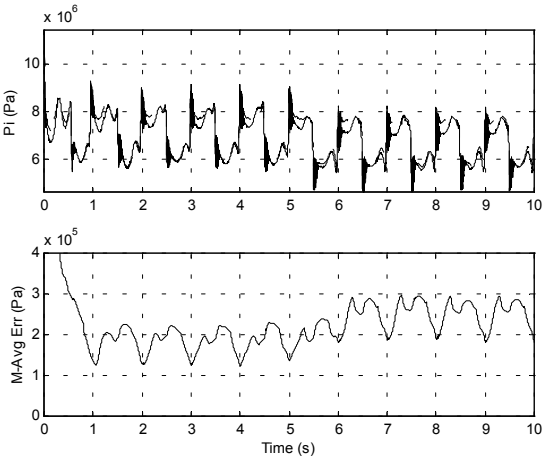

Fig. 6: Cylinder chamber pressure P_i with external leakage level I on P_i side

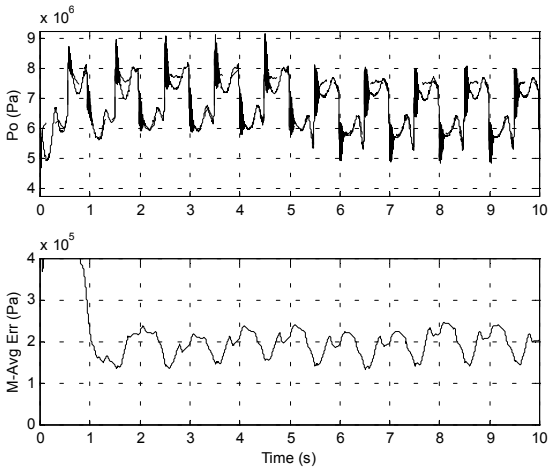

Fig. 7: Cylinder chamber pressure P_o with external leakage level I on P_i side

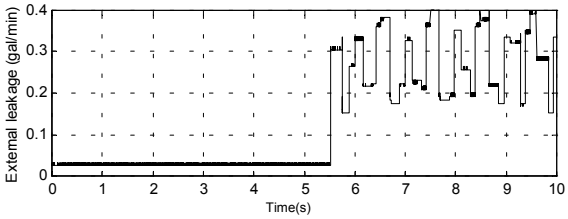

Fig. 8: External leakage, level II

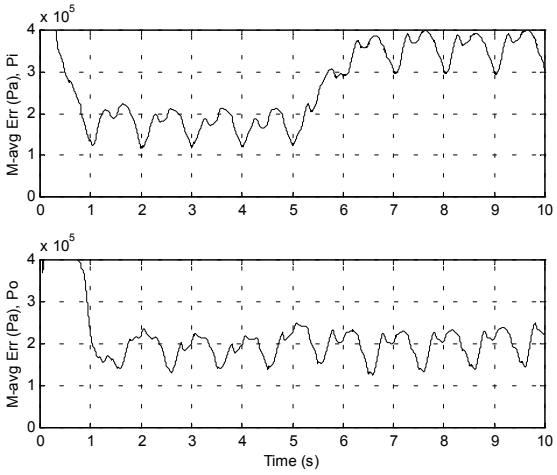

Fig. 9: Cylinder chamber pressures P_i and P_o with external leakage level II on P_i side

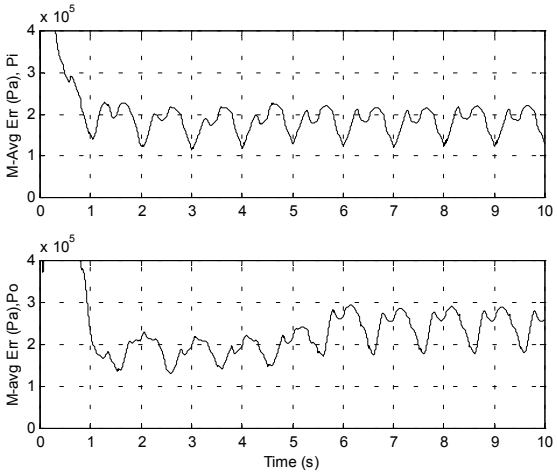

Fig. 10: Cylinder chamber pressures P_i and P_o with external leakage level I on P_o side

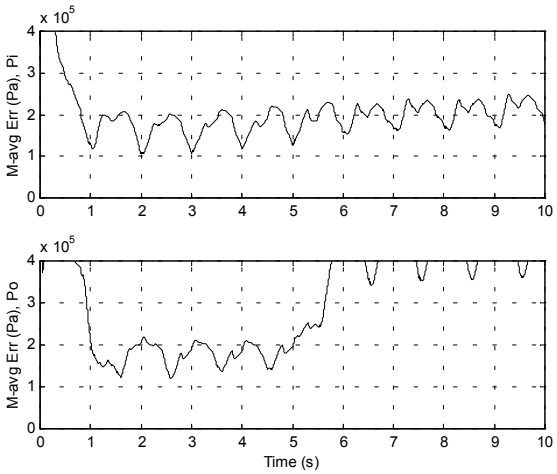

Fig. 11: Cylinder chamber pressures P_i and P_o with external leakage level II on P_o side

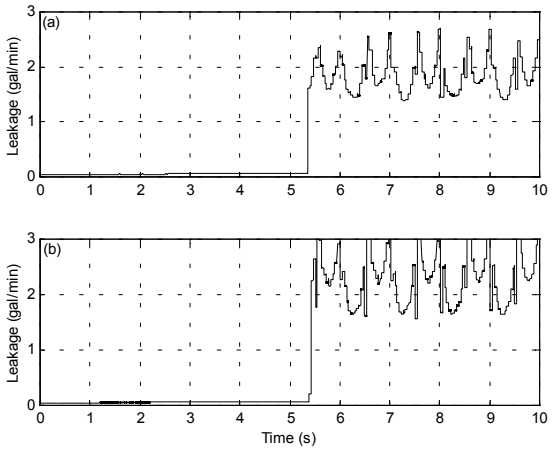

Fig. 12: Internal leakage, level I(a) and II(b)

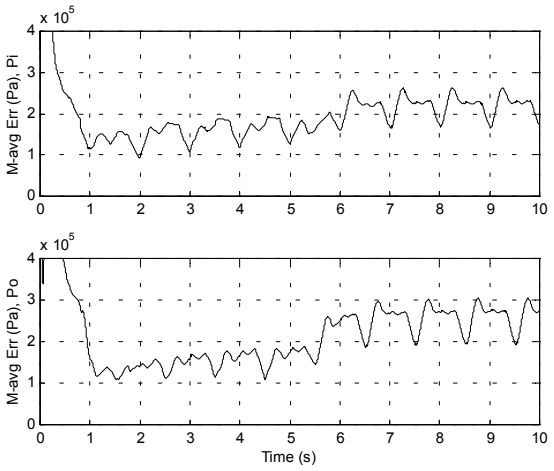

Fig. 13: Cylinder chamber pressures P_i and P_o with internal leakage level I

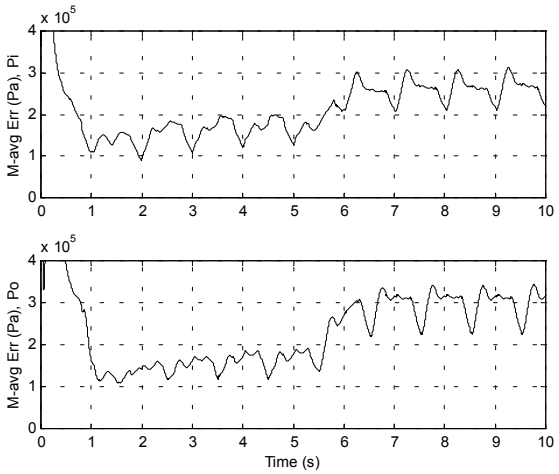

Fig. 14: Cylinder chamber pressures P_i and P_o with internal leakage level II